

Turbulent Convection and Pulsational Stability of Variable Stars

II. Oscillations of RR Lyrae and Horizontal Branch Red Variable Stars

D. R. Xiong¹, Q. L. Cheng¹ & L. Deng²

¹Purple Mountain Observatory, Academia Sinica, Nanjing 210008, P.R. China

²Beijing Astronomical Observatory, Academia Sinica, Beijing 100080, P.R. China

ABSTRACT

Using a nonlocal time-dependent theory of convection, we have calculated the linear non-adiabatic oscillations of the Horizontal Branch (HB) stars, with both the dynamic and thermodynamic coupling between convection and oscillations carefully treated. Turbulent pressure and turbulent viscosity have been included consistently in our equations of non-adiabatic pulsation. When the coupling between convection and oscillations is ignored, for all models with $T_e \leq 7350$, the fundamental through the second overtone are pulsationally unstable; while for $T_e \leq 6200$ all the models are unstable up to (at least) the 9th overtone. When the coupling between convection and oscillations is included, the RR Lyrae instability strip is very well predicted. Within the strip the most models are pulsationally unstable only for the fundamental and the first few overtones. The turbulent viscosity is an important damping mechanism. Being exclusively distinct from the luminous red variables (long period variables), the HB stars to the right of the RR strip are pulsationally stable for the fundamental and low-order overtones, but become unstable for some of the high-order overtones. This may provide a valuable clue for the short period, low amplitude red variables found outside the red edge of the RR strip on the H-R diagram of globular clusters. Moreover, we present a new radiation modulated excitation mechanism functioning in a zone of radiation flux gradient. The effects of nonlocal convection and the dynamic coupling between convection and oscillations are discussed. The spatial oscillations of the thermal variables in the pulsational calculations have been effectively suppressed.

Subject headings: Convection - stars: horizontal branch - stars: Oscillation - stars: variables; RR Lyrae

1. Introduction

The main goal of the series of our present work is to study the effects of convection on the stability of variable stars of different types. Gough (1977) and Xiong(1977) have pointed out independently that a nonlocal time-dependent theory of convection is needed in order to account for the dynamic coupling between convection and oscillations. Based on the general equations of

fluid dynamics and the theory of turbulence, we have developed such a nonlocal time-dependent statistical theory of convection (Xiong, Cheng & Deng 1997), which gives an equation for turbulent viscosity that is formally similar to the Stokes equation for viscous gas. The theoretical reasonings and the correct expression of the gradient approximation for the triple correlations (the 3rd-order correlation functions of the turbulent fluctuations of velocity and temperature) are provided by the dynamic equations. We have presented results of the linear nonadiabatic oscillations for long period variables in the first paper of this series (Xiong, Deng & Cheng, 1997, hereafter Paper I), in which a so-called Mira instability region outside the Cepheid instability strip has been defined. In this paper, we will apply our theory to the study of the pulsational stability of HB stars.

The theoretical progress of RR Lyrae star research is due to many authors, among which we recall Christy (1966), Iben (1971), Baker and Gough (1979), Deupree (1977a,b,c), Xiong (1980), Stellingwerf (1984), Bono and Stellingwerf (1993), Guzik and Cox (1993) and Bono et al (1995, 1997). Christy(1966) and Iben(1971) completely ignored the coupling between convection and oscillations, therefore they gave no definition for the red edge of the RR instability strip. Baker & Gough (1979) followed Gough’s local time-dependent mixing length theory of convection (Gough 1977), while Xiong (1980) used a local time-dependent statistical theory of convection (Xiong 1977). The later two papers gave very close results, and both reached a definite red edge of the RR instability strip. The detailed comparison of the two was given by Balmforth & Gough (1987). The coupling between convection and oscillations was attempted by Stellingwerf (1984) and Bono et al (1993, 1995, 1997) using a rather simplified nonlocal time-dependent theory of convection. In this paper, we have put great emphasis on the theoretical baseline of the convection theory, using which we have calculated the linear non-adiabatic pulsation for RR Lyrae stars. We are going to show the advantages of the present theory over the local time-dependent theory of convection.

It is claimed that a bunch of short period, small amplitude variables were found outside the RR instability strip on the H-R diagram of some globular clusters (Yao 1981, 1986, 1987; Yao et al. 1993a,b, 1994). In this paper we try to give a theoretical interpretation of such variables. In the following section, the main results of the calculated models for non-adiabatic pulsation are presented. We also proposed a new excitation mechanism, i.e. the so called “radiation modulated excitation mechanism”, which works in the region of radiation flux gradient. We have explained in Section 3 the reason for the spatial oscillations of the thermodynamic quantities that happen in the numerical computations of stellar pulsation . A concise discussion and conclusions of our work are in Section 4

2. The Numerical Results

We have calculated the fundamental through 11th order overtone modes of linear non-adiabatic oscillations for six series of HB star models with a intermediate metal abundance. All the model series have the same chemical composition: $(X, Z) = (0.76, 0.0004)$. Their mass, luminosity, chemical composition and the characteristics of pulsational instability region are listed in Table 1.

The model parameters are: $M = (0.65 - 0.80)M_{\odot}$; $L = (1.5 - 2.2) \times 10^{35} \text{ erg/s}$ ($M_{bol} = 0.77 - 0.35$); and effective temperature in the range of $5150 - 8075K$, where the coolest model is very close to the Hayashi track; the convection parameters $c_1 = c_2 = 0.75 - 1.00$, which correspond to the same energy transport efficiency as taking $\alpha = l/H_p \approx 1.5 - 2.0$ in the original Vitense theory, and the e-folding length of convective overshooting of about $(1.05 - 1.4)H_p$. The coupling between convection and oscillations is carefully treated by using our nonlocal time-dependent theory of convection (Xiong, 1989, Xiong, Cheng & Deng 1997). All the mathematical and numerical schemes are the same as in Paper I to which we refer for all the details in the equations and boundary conditions.

The lower boundary is set in the convective overshooting zone ($T = 8 \times 10^6 K$), and the upper one is set optically thin enough in the stellar atmosphere (optical depth $\tau = 0.01$). We use a simplified MHD equation of state (Hummer and Mihalas, 1988; Mihalas et al. 1988; Dappen et al. 1988) in the present work. An analytic approach to the OPAL tabular opacities (Rogers and Iglesias 1992) and the low-temperature tabular opacities (Alexander 1975) is used for the calculation of opacity. The Henyey method (Henyey et al. 1964) is used for numerical calculations. The envelope model of stars is divided into 800 zones with approximately equal intervals in $\ln T$. However, the mesh points have been increased in the stellar atmosphere, where the temperature gradient is very small. The variations of the temperature and pressure within any mesh zone are less than 0.03 dex. These mesh points have enough spatial resolution for the highest overtone in the present work. The eigen-functions of the 10th overtone for a red HB model are plotted in Fig. 1.

2.1. Radiative Modulation Excitation

In order to demonstrate the effects of convection on the stability of stellar pulsation, we have considered separately two cases, i.e. including and ignoring the coupling between convection and oscillations (however, convection has been included in the calculation of equilibrium models). The treatment of decoupling can be referred to Paper 1. Simply saying, it is by setting the convective variables to zero. Table 2 gives the linear amplitude growth rates for the first 12 eigen-modes for the case that the coupling between convection and oscillations is ignored. The first column is the serial number of the model, the second is the effective temperature T_e , 3rd – 14th columns are respectively the amplitude growth rates for the fundamental to the eleventh overtone. As it is clear from Table 2, for all models with $T_e \leq 7325$, the fundamental through the second overtone are pulsationally unstable; while all the models with $T_e \leq 6200$ K are unstable up to (at least) the 9th overtone. This makes it clear that the red edge of the RR instability strip cannot be determined when the coupling between convection and oscillations is ignored. Fig. 2a-f depicts the variation of the integrated work versus the depth ($\log T$) for six HB stellar models with different effective temperatures.

It can be seen from Fig. 2 that the excitation of pulsation mainly comes from 3 regions,

namely, the κ mechanism (KM) which works in the vicinity of the helium and hydrogen ionization regions, and the modulation excitation mechanism working in the gradient zones of radiation flux (RGZ) on the top and at the bottom of convection zone, about which we are going to talk in details below. For the HB stars with $T_e \leq 5800K$, the ionization region of helium is almost completely convective and the radiation energy transport is nearly negligible ($L_r/L < 1\%$). Therefore, the KM working near the hydrogen and helium ionization regions is not at all important. The pulsation is excited by the KM and the radiation modulated excitation (RME) mechanism above the hydrogen ionization region, where $dW_p/d\log T < 0$ (Fig. 2a,b). There is a lot of work concentrated on the KM in the literature. We will focus on the new mechanism of pulsational excitation, i.e. the modulation excitation that works in the RGZ on the top and at the bottom of the convective zone. In such RGZ the radiation flux will be modulated when the star pulsates. The function of such modulation is to gain energy from the surroundings through radiation while the fluid element is hot, and to loss energy while it is cool. Thus on the P-V work plot, a positive Carnot cycle forms, that is to say, radiation energy is converted into pulsational kinetic energy by such a process. In the following, we are going to explain how such an excitation mechanism works by using the integrated work. Following our previous work (Cheng & Xiong 1997), the normalized integrated work can be expressed as

$$W_P = -\frac{\pi}{2E_k} \int_{M_b}^{M_0} \frac{1}{\rho^2} I_m (\delta P \delta \rho^*) dM_r, \quad (1)$$

where, E_k is the total kinetic energy of oscillations,

$$E_k = \frac{1}{2} \omega_r^2 \int_{M_b}^{M_0} \delta r \delta r^* dM_r, \quad (2)$$

Starting from the equation of conservation of energy, one can easily have,

$$\frac{dP}{dt} - \Gamma_1 \frac{P}{\rho} \frac{d\rho}{dt} = -(\Gamma_3 - 1) \rho \frac{d}{dM_r} (L_r + L_c + L_t), \quad (3)$$

where L_r , L_c and L_t are respectively the corresponding luminosities of the radiative, convective and turbulent kinetic energy fluxes. Inside the equilibrium model of stellar envelope,

$$L_r + L_c + L_t = L = \text{const.} \quad (4)$$

Linearizing Eq. (3), we have

$$\delta P = \Gamma_1 \frac{P}{\rho} \delta \rho - (\Gamma_3 - 1) \frac{\rho}{i\omega} \frac{d}{dM_r} (\delta L_r + \delta L_c + \delta L_t), \quad (5)$$

Inserting Eq. (5) into Eq. (1), we have

$$W_P = -\frac{\pi}{2\omega_r E_k} \int_{M_b}^{M_0} R_e \left\{ (\Gamma_3 - 1) \frac{\delta\rho^*}{\rho} \frac{d}{dM_r} (\delta L_r + \delta L_c + \delta L_t) \right\} dM_r. \quad (6)$$

For not losing any generality and for the sake of convenience in discussing the coupling between convection and oscillations, we have kept in Eqs. (5) and (6) the terms related with convection, i.e. δL_c and δL_t . If δL_c and δL_t are set to zero, this will lead to exclusion of the coupling between convection and oscillations. We note

$$\frac{\delta L_r}{L_r} = \frac{d}{d \ln T} \left(\frac{\delta T}{T} \right) + (4 - \chi_T) \frac{\delta T}{T} - \chi_P \frac{\delta P}{P} + 4 \frac{\delta r}{r}, \quad (7)$$

$$\frac{\delta L_c}{L_c} = (\delta + C_{p,P}) \frac{\delta P}{P} + (1 + C_{p,T} - \alpha) \frac{\delta T}{T} + 2 \frac{\delta r}{r} + \frac{\delta V}{V}, \quad (8)$$

$$\frac{\delta L_t}{L_t} = \frac{\delta L_1}{L_1}, \quad (9)$$

$$(\Gamma_3 - 1) \frac{\delta\rho^*}{\rho} \approx \frac{\delta T^*}{T}, \quad (10)$$

$$\frac{\delta P}{P} \approx \frac{\Gamma_2}{\Gamma_2 - 1} \frac{\delta T^*}{T}, \quad (11)$$

where α and δ are the coefficients of expansion and compression of gas. Putting Eqs. (7) - (11) into Eq. (6), W_P can be expressed as a sum of the following five terms

$$W_P = W_{KM} + W_{RME} + W_{CE} + W_{CME} + W_{L_t}, \quad (12)$$

where W_{KM} and W_{RME} are the contributions of the normal KM and RME respectively,

$$W_{KM} = \frac{\pi}{2\omega_r E_k} \int_{r_b}^{R_0} R_e \left\{ \frac{\delta T^*}{T} \frac{d}{dr} \left[\left(\chi_T + \frac{\Gamma_2}{\Gamma_2 - 1} \chi_P - 4 \right) \frac{\delta T}{T} - \frac{d}{d \ln T} \left(\frac{\delta T}{T} \right) - 4 \frac{\delta r}{r} \right] L_r \right\} dr, \quad (13)$$

$$W_{RME} = \frac{\pi}{2\omega_r E_k} \int_{r_b}^{R_0} R_e \left\{ \frac{\delta T^*}{T} \left[\left(\chi_T + \frac{\Gamma_2}{\Gamma_2 - 1} \chi_P - 4 \right) \frac{\delta T}{T} - \frac{d}{d \ln T} \left(\frac{\delta T}{T} \right) - 4 \frac{\delta r}{r} \right] \frac{dL_r}{dr} \right\} dr, \quad (14)$$

W_{CE} and W_{CME} are the contributions of the convective thermal flux and the convective (flux) modulation excitation (CME),

$$W_{CE} = -\frac{\pi}{2\omega_r E_k} \int_{r_b}^{R_0} R_e \left\{ \frac{\delta T^*}{T} \frac{d}{dr} \left[\left(1 + C_{p,T} - \alpha + \frac{\Gamma_2}{\Gamma_2 - 1} (\delta + C_{p,P}) \right) \frac{\delta T}{T} + 2 \frac{\delta r}{r} + \frac{\delta V}{V} \right] L_c \right\} dr, \quad (15)$$

$$W_{CME} = -\frac{\pi}{2\omega_r E_k} \int_{r_b}^{R_0} R_e \left\{ \frac{\delta T^*}{T} \left[\left(1 + C_{p,T} - \alpha + \frac{\Gamma_2}{\Gamma_2 - 1} (\delta + C_{p,P}) \right) \frac{\delta T}{T} + 2 \frac{\delta r}{r} + \frac{\delta V}{V} \right] \frac{dL_c}{dr} \right\} dr, \quad (16)$$

and W_{Lt} is the contribution of the turbulent kinetic energy flux,

$$W_{Lt} = -\frac{3\pi}{2\omega_r E_k} \int_{r_b}^{R_0} R_e \left\{ \frac{\delta T^*}{T} \left[L_1 \frac{d}{dr} \left(\frac{\delta L_1}{L_1} \right) + \frac{\delta L_1}{L_1} \frac{dL_1}{dr} \right] \right\} dr. \quad (17)$$

In our nonlocal convection theory $|L_1/L| \ll 1$, so W_{Lt} is negligible in comparison with W_{KM} , W_{RME} , W_{CE} and W_{CME} .

When $d\{[\chi_T + \chi_P \Gamma_2 / (\Gamma_2 - 1) - 4] |\delta T/T|\} / dr > 0$ (< 0), KM plays a destability (stability) effect for stellar oscillations. The destability effect is enhanced in the hydrogen and helium ionization regions, because Γ_2 is small due to the ionization of hydrogen and helium (Gamma mechanism). When the coupling between convection and oscillations is ignored, $W_{CE} = W_{CME} = 0$ and $W_P = W_{KM} + W_{RME}$. This theoretical prediction has been justified by our numerical calculations.

The integrated works W_{KM} and W_{RME} are also plotted in Fig. 2. It can be seen from Fig. 2 that in the stellar interior, where the pulsational amplitudes increase outwards, the W_{KM} increases (decreases) with increase (decrease) of κ_T .

There is a radiative damping region ($dW_P/d\log T > 0$) in the deep radiative interior, where $W_{KM} < 0$. For stars with very low effective temperature, such a radiative region goes even deeper into the stellar interior where the pulsational amplitude is small, and the radiative damping is small as well, as this is seen in Fig. 2a,b. As the temperature increases, the envelope convective zone retreats towards the surface. The radiative damping region progresses outwards, and the radiative damping increases (Fig. 2c-f). There is also a radiative damping region ($dW_{KM}/d\log T > 0$) in the stellar atmosphere, because the pulsational amplitude of $\delta T/T$ decreases towards surface.

The RME exists only in the RGZ. In a stellar envelope RGZ is present only at the top and the bottom of the convective zone [Up Radiative Gradient Zone (URGZ) and Bottom Radiative Gradient Zone (BRGZ)]. In the BRGZ where $dL_r/dr < 0$ and $\chi_T + \chi_P \Gamma_2 / (\Gamma_2 - 1) - 4 < 0$, W_{RME} is positive. Therefore, the BRGZ is an excitation region of oscillations (Fig. 2b-e). In the URGZ the above two inequalities are both reversed. This is another excitation region (Fig. 2a-d). Such an excitation mechanism is related to opacity κ , but it is distinct from the normal KM. The normal KM can work in purely radiative stellar configuration, for example, such as the excitation of β Cephei variables, which have almost no convection zone. This new exciting mechanism, however, works only in the RGZ. We will call it the radiation modulated excitation (RME), so as to distinguish it from the normal KM.

The location of the RME at the top of a convective zone overlaps with that of the normal KM, so it is difficult to distinguish them in the total power diagram ($W_P - \log T$). But, they are clearly distinguished with the curves of W_{KM} and W_{RME} . The location and the efficiency of the RME

at the bottom of the convective zone depend very sensitively on the effective temperature of the stellar model under consideration. For extremely low temperature models, the envelope convective zone is very extended, and this leads to a very deep modulated excitation region at the bottom of the convective zone. However, the pulsational amplitude in this region is very small, so a very weak excitation is expected. The main excitation comes from the KM and RME mechanisms in the URZ (Fig. 2a,b) for the cool HB stars. In Fig. 2b, the bottom RME is only barely visible. As the effective temperature increases, the bottom RME raises up together with the shrinking of the convective zone (Fig. 2a-d). The effect of bottom RME is clearly illustrated in Fig 2b and Fig 2c. The bottom RME starts to work at $\log T \approx 5.7$ and 5.4 respectively, corresponding to the location of the bottom of the convective zone and being much lower than the second ionization region of helium where the normal KM works. For a HB star with $T_e = 5900$ the bottom RME region is connected or overlaps with the second ionization region of helium (Fig. 2c). Numerically, RME is stronger than the KM in the second ionization region of helium. For models with $T_e = 6200K$ the bottom RME region is near the second ionization region of helium (Fig. 2d). From the total power diagram ($W_P - \log T$) it is difficult to distinguish the RME from the KM. The effects of RME still can be seen from the large increase of integrated work W_{RME} near $\log T = 4.8$ corresponding to the location of the bottom of the convective zone.

For the blue HB stars, the convective energy transport is insignificant since the convective envelope is very shallow, and the KM functioning in the second ionization region of helium becomes dominant, while RME is almost not at all working. We can also see from Fig. 2f that the excitation due to the KM cannot balance the radiative damping in deeper layers for high enough effective temperature models and the star becomes pulsationally stable. This is the reason of the existence of the blue edge of the RR instability strip.

One can see from Fig. 2 that there is a bump near $\log T \approx 5.3$. It results from the bump of the new OPAL opacity.

2.2. The RR Instability Strip

As we have repeatedly stressed, when the coupling between convection and oscillations is ignored, all the HB star models with $T_e \leq 7550K$ are pulsationally unstable. Therefore, no definition for the red edge of RR strip can be given. However, when the coupling is taken into consideration, the situation becomes very promising. We have listed in Table 3 the linear amplitude growth rates of pulsation (per period) for the first twelve modes. From this table we find that when the coupling between convection and oscillations is considered, the fundamental and low-order overtones ($n \leq 3$) become pulsationally stable for all the HB stellar models with $T_e \leq 5940$. Namely, there is an apparent red edge of the RR instability strip. The amplitude growth rates of the fundamental and the first overtone versus the effective temperatures for the model series 2 - 4 are plotted in Fig. 3. In Fig. 4 the integrated works versus depth are given for the fundamental modes of 6 HB stellar models, where W_P , W_{Pt} and W_{vis} are, respectively,

the contributions due to the gas (including radiation), turbulent pressure and turbulent viscosity, while $W_{all} = W_P + W_{Pt} + W_{vis}$ is the total integrated work, the numerical value of which at the surface is approximately the same as the linear pulsational amplitude growth rate $\eta = -2\pi\omega_i/\omega_r$ computed with the non-adiabatic scheme. Here ω_i and ω_r are the imaginary and real part of the complex pulsational angular frequency ($\omega = i\omega_i + \omega_r$). For the real definitions of W_P , W_{Pt} and W_{vis} we refer to our previous work (Cheng & Xiong 1997). Here we only recall that of W_{vis} to make our discussion clearer. $-W_{vis}$ is the random turbulent kinetic energy converted from the pulsational energy due to turbulent viscosity, which is finally turned into thermal energy through molecular viscous processes. W_{vis} is always negative. Therefore, This implies a damping mechanism.

We can see from Fig. 4 that, for HB models with $T_e \geq 6000K$, the radiation energy transport is becoming dominant gradually in their second ionization region of helium. For these stars, the main source of excitation is the KM in the second ionization region. When the effective temperature drops below $5900K$ for the HB models, the hydrogen and helium ionization regions are fully convective, and the radiation contributes very little to the total energy flux ($L_r/L \leq 1\%$). Therefore, the KM is almost inhibited. The convection becomes the dominant factor for determination of the pulsational stability of stars. Thus, the low temperature HB stars with $T_e \leq 5940K$ become pulsationally stable. The coupling between convection and oscillations is the cause why there exists a red edge for the RR Lyrae instability strip. Fig 6 plots the variations of temperature for the lower boundaries of the convective zone and the ionization regions of hydrogen and helium versus the effective temperature of the HB models under consideration. As demonstrated in Fig. 6, the red edge of the RR Lyrae instability strip is defined when the bottom of the convective zone is just extended slightly below the second ionization region of helium.

2.3. The Short Period Red Variables Beyond the RR Lyrae Strip

Yao and his collaborators found some short period red variables outside the RR Lyrae strip in the H-R diagrams of a few globular clusters (Yao 1981, 1986, 1987; Yao et al 1993a,b, 1994). The light amplitude of such red variables is as small as a few percent of a magnitude. These stars are usually multi-periodic or irregular; their typical period or the time-scale of variability is a few tenths of a day. Taking the variation of light of such red variables as a result of intrinsic pulsation, the natural conclusion is that the stars all pulsate at high-order overtones. In general, the dwarfs tend to be non-radially excited while the giants are radially excited. Therefore, we think that the short period red variables are pulsating in high radial overtones. Of course, we cannot exclude the possibility that they pulsate at low degree non-radial modes. It is very interesting to see from Table 3 that, when the coupling between convection and oscillations is considered, all the fundamental and low-order overtones of the red HB models for $T_e \leq 5940K$ are pulsationally stable; while some high-order overtones ($n \geq 4$) are pulsationally unstable. We also show that these low temperature red variables possess nearly the same period as that of the variables found

to right side of the RR Lyrae strip by Yao and his collaborators. A general regularity of variable stars is that when a star pulsates at high-order overtones, its pulsation amplitude is usually very small and tends to be multi-periodic. The results of our theoretical modeling are likely to be a reasonable explanation for the red variables found outside the RR Lyrae strip in globular clusters and for their qualitative properties, though there still exist some questions to be studied. According to our theory, it seems that all the low temperature HB stars ought to be pulsationally unstable at high-order overtones. This raises a naive question: why these short period oscillations were observed only for some, not for all the low temperature HB stars? A straightforward answer to such a question is that they all might be pulsationally unstable but are not detectable with current instrumental precision. This seems to be a reasonable answer. However, there is still a question to be asked: what is the drive to make some of the stars pulsate with higher amplitudes? We are not ready to give satisfactory explanations to such questions.

2.4. Comparison with Other Theoretical Results and Observations

The RR Lyrae instability strip yielded by our numerical computations of the linear non-adiabatic oscillations is $3.774 \leq \log T_e \leq 3.884$ for the second model series ($c_1 = c_2 = 0.85$). The location of instability strip of the fundamental mode agrees well with Bono’s nonlinear theoretical results (Bono, et al. 1997). The temperature of the red edge for the fundamental mode is slightly higher, while the temperature of the blue edge is slightly lower than theirs. Our blue edge of the first overtone is much hotter than that given by Bone’s nonlinear results. Their blue edge, we think, seems to be too red. Our theoretical red edge of the first overtone is slightly hotter than the fundamental mode red edge. Obviously, it is too red in comparison with observations. It is the intrinsic defect of the linear theory. This is a problem of mode choice. It is impossible to decide which mode can finally become an unstable one with limited amplitude for the linear theory when several modes are linearly pulsationally unstable.

For the globular cluster M3 whose metallicity is close to what we adopted in this work. Sandage (1990) determined observationally a RR Lyrae instability strip $3.791 \leq \log T_e \leq 3.880$. This infers that the theoretical result matches very well the observed one for the blue edge of the instability strip, while the red edge is 240 K lower than the observed one. For the same mass, luminosity, effective temeperatute and chemical composition, the convection zone deepens as c_1 increases. Therefore, the location of the red edge of the instability strip can be adjusted by modifying the convective parameter c_1 . We calculated the linear non-adiabatic oscillations of three series of HB star models with different c_1 . The effective temperatures of the blue and red edges for the fundamental and the first overtone are listed in Table 1. The red edge is still 170 K lower than observation even when c_1 is increased to 1.0. The energy transport efficiency in this case corresponds to that of taking $\alpha = l/H_p \approx 2.0$ in the original Vitense theory. It seems impossible that c_1 can be much larger than 1. We do not know whether this is due to the imperfection of our theory or because the temperature of the red edge determined by Sandage is too high.

2.5. Luminous Red Variables (LRV) and Red HB Stars (RHBS)

Although LRV and RHBS are in the different evolutionary statuses, they all possess very extended convective envelopes. Convection is the most dominant factor controlling their pulsational stability. However, their pulsational properties are entirely different: LRV are pulsating at the fundamental and the first few overtones, while all higher ($n > 4$) overtones are stable. On the contrary, for RHBS the fundamental and lower order overtones ($n \lesssim 4$) are pulsationally stable, while some higher order overtones are unstable. It is hard to understand this acute difference at the first glance. In fact, this is because these two types of stars have quite different mass-luminosity ratios: The masses of LRV do not differ much from those of RHBS, while the luminosities of LRV are higher than those of RHBS up to 2 orders of magnitude. Thus their mass-luminosity ratios differ about in 2 orders of magnitude. This implies that the envelope structure of LRV is very different from that of RHBS. For LRV, the central condensation is very high. This will lead to very different pulsational properties for these two types:

1. An important factor is that the thermal time scales of pulsational amplitude growth for these two types are very different, and this is due to the tremendous difference of mass-luminosity ratios. According to Eq. (4) in Paper I, this thermal time scale can be expressed as $4\pi r^3 \rho C_p T / L$. Since the luminosity of LRV is high and the gaseous density in their envelope is very low in comparison with RHBS, the thermal time scale of LRV is very short (compared with their pulsation period). It has been shown by actual calculations that the amplitude growth rate (the amplitude increment in a pulsational period) of LRV is higher than that of RHBS by about 2–3 orders of magnitude. This means that, for LRV, the excitation (damping) by radiative (and convective) energy transport is very strong. Therefore, for fundamental and low-order overtones, the effect of turbulent viscosity will be relatively weak (please refer to Fig. 3 in Paper I). Besides, LRV will tend to pulsate at fundamental and low-order overtones because $\omega\tau_c \ll 1$ in most regions of LRV interiors. Here τ_c is the convective inertial time scale. As the frequency increases, the effects of turbulent viscosity increase rapidly [the turbulent viscosity is proportional to $\omega\tau_c / (1 + \omega^2\tau_c^2)$]. Thus their high overtones tend to be pulsationally stable (please refer to Fig. 4 in Paper I). For RHBS, since the amplitude growth rates are about 2–3 orders of magnitude less than those of LRV, the effects of turbulent viscosity become relatively important (see Fig. 4), and will damp the pulsation. The tremendous difference of mass-luminosity ratios is another reason for the distinct properties of the two types of low temperature variables.
2. The distributions of $\omega\tau_c$ are totally different in the interiors of these two types. In fact, the interaction between convection and oscillations is very complicated. The effects of convection on stellar pulsation depend not only on the variation amplitudes of convective variables, but also on their relative phases. Both the amplitude and phase depend critically on the ratio of convective inertial time scale (τ_c) and that of pulsation, i.e. $\omega\tau_c$. Comparing the integrated work plot of the present work (Fig. 4) with that of long period variables in our previous paper

(Paper I), we can see that, the quantity $\omega\tau_c$ is very different in the interiors of these two types of stars. For the LRV, $\omega\tau_c < 1$ in most part of the stellar interior except the very outer part near stellar surface; while for the RHBS $\omega\tau_c \gg 1$ in almost the whole stellar interior. Referring to Fig 3 of our previous work (Paper I), it is clear that the hydrogen and helium first ionization regions are the main excitation region of stellar pulsation for the LRV, where convection tends to destabilize pulsation, while the turbulent viscosity is the main damping mechanism for high-order overtones, due to turbulent viscous dissipation ($\propto \omega\tau_c/(1 + \omega_r^2\tau_c^2)$). When $\omega\tau_c \ll 1$, the turbulent viscosity is proportional to $\omega\tau_c$, which increases very quickly with increasing pulsational frequency. It becomes opposite for the RHBS, for which $\omega\tau_c \gg 1$ holds in most part of the stellar interior. The excitation due to the first ionization region of helium and a part of ionization region of hydrogen is restrained, and the damping effect of turbulent viscosity on high-order overtones also diminishes. This tends to stabilize the fundamental and the low-order overtones of the RHBS while the high-order overtones become pulsationally unstable. Following such discussion we conclude that the difference in $\omega\tau_c$ is a reason for the distinct properties of the two types of low temperature variables. As for the question of why $\omega\tau_c$'s are so different in the two type of stars, we understand that it is due to the convective inertial time scale $\tau_c \propto H_P/x$. Here $H_P = r^2P/GM_r\rho \propto r^2P/M_r\rho$ is the local pressure scale height and x is the r.m.s. component of the turbulent velocity. Relative to the RHBS, the LRV have higher central condensation. Towards stellar center, r goes much faster with increasing temperature. Fig. 6 plots r , H_P and $\omega\tau_c$ of fundamental mode versus temperature for a RHBS model and a LRV model respectively. It is clearly shown in Fig. 7 that there exists very large difference between the two types of low temperature variables of different luminosities. Following the above discussion, we can easily understand the reason of the distinct properties of the two types of low temperature variables although their variabilities are both affected critically by convection. Fig. 5 plots the variations of the integrated work of the first, second, and fourth overtones versus depth for a $T_e = 5150K$ RHBS model. From this we see that, unlike luminous red stars, the turbulent viscosity component W_{vis} does not increase quickly with ω_r .

3. The Spatial Oscillations of the Convective Variables

In the theoretical calculation of the steller oscillations, if the local theory is used to treat the coupling between the convection and pulsation, the troublesome spatial oscillations of thermodynamic variables will occur (Keeley, 1977; Baker and Gough, 1979; Gonczi and Osaki, 1980). These spatial oscillations are due to the local treatment of the convection, so we could expect that it will automatically disappear if the non-local treatment of convection is adopted. Unfortunately, there still exist intense spatial oscillations of convective and thermodynamic variables in our previous work on the solar radial p-mode oscillations, although a non-local convection theory was used (Cheng and Xiong, 1997). Now, we use an asymptotic analysis to inspect the cause of spatial oscillations. It is necessary to review briefly the main points of our

non-local convection theory first. Our convection theory is a statistical theory of correlation functions. We derived a set of dynamic equations of the auto- and cross-correlations of the turbulent velocity and temperature fluctuations. For example, the dynamic equation for the auto-correlations of the turbulent velocity is as follows (Xiong, Deng and Cheng, 1997),

$$\begin{aligned} & \frac{D}{Dt} \overline{w'^i w'^j} + \overline{w'^i w'^k} \nabla_k \bar{w}^j + \overline{w'^j w'^k} \nabla_k \bar{w}^i \\ & - \alpha \left(g^{ik} \frac{\overline{w'^j T'}}{\bar{T}} + g^{jk} \frac{\overline{w'^i T'}}{\bar{T}} \right) \left(\nabla_k \bar{\Phi} + \frac{D\bar{u}_k}{Dt} \right) \\ & + \bar{\rho} \nabla_k (\overline{\rho u'^k w'^i w'^j}) = -4\sqrt{3}\eta_e x \overline{w'^i w'^j} / l_e, \end{aligned} \quad (18)$$

where $x = \sqrt{\overline{w'_i w'^i}}/3$ and l_e is the average size of the energy-containing eddies. We assume that $l_e \sim c_1 H_p$ (H_p is the local pressure scale height). The right-hand side term of Eq. (18) is the turbulent dissipation, which determines the efficiency of the convective energy transport. Thus, c_1 , which is a convective parameter relevant to the turbulent dissipation, functions like the parameter $\alpha = l/H_p$ in the mixing-length theory (Bohm-Vitense, Z. 1958). In our theory, the efficiency of the convective energy transport is approximately the same as letting $\alpha = l/H_p = 2c_1$ in the original mixing-length theory.

$\overline{\rho w'^i w'^j}$ is the turbulent Reynold stress. We can decompose it into an isotropic component (turbulent pressure) and a nonisotropic one (turbulent viscosity). An expression for the turbulent viscosity very similar in form to the formula of Stokes viscosity has been derived (Xiong, Deng and Cheng, 1997). To reveal the nature of the non-local convection, we consider only the isotropic component of Eq. (18), i.e.

$$\begin{aligned} & \frac{3}{2} \frac{Dx^2}{Dt} = -x^2 \nabla_k \bar{u}^k + \alpha V^k \left(\frac{D\bar{u}_k}{Dt} + \nabla_k \bar{\Phi} \right) \\ & + \bar{\rho} \nabla_k (\overline{\rho u'^k w'_i w'^i}) - 2\sqrt{3}\eta_e x^3 / l_e, \end{aligned} \quad (19)$$

where $V^k = \overline{w'^k T'}/bT$ embodies the correlation of the turbulent velocity and temperature fluctuations. Eq. (19) is the dynamic equation of turbulent pressure. But it can also be considered as the equation of conservation of turbulent kinetic energy. The left-hand side of Eq. (19) is the rate of turbulent kinetic energy, which equals the sum of the terms on the right-hand side. The first one is the rate of regular kinetic energy of average motion converted to turbulent kinetic energy. The second term is the rate of thermal energy converted to turbulent kinetic energy through the work done by buoyancy. The last term is the rate of turbulent kinetic energy converted to thermal energy due to the molecular viscosity. The triple correlations in the brackets of the third term are the turbulent kinetic flux, which represents the non-local turbulent kinetic

energy transport by convection. These triple correlations represent all the effects of non-local convection. They reveal the essential difference between local and non-local theory: If one ignores all the triple correlations, the theory will return to the local convection theory (Xiong, 1977). In our earliest works, we used a simplified gradient-type diffusion approximation (Xiong,1979), i.e.

$$\overline{u'_k w'_i w'^i} = -lx \nabla_k \overline{w'_i w'^i} = -3lx \nabla_k x^2, \quad (20)$$

where l is the diffusion length. We assume $l = c_2 \sqrt{3} H_p / 4$. c_2 is another convective parameter relevant to the non-local turbulent diffusion. The e-folding length of convective overshooting is about $1.4 \sqrt{c_1 c_2} H_p$. Let $c_2 = 0$, then we get back to local convection theory.

Eq. (20) is introduced only as a physically reasonable assumption. Recently, we have derived a set of dynamic equations for triple correlations (Xiong, Deng and Cheng, 1997). These equations are very complex: The complete set of the radiative fluid dynamic equations are up to the 14th order. In the dynamic equations for triple correlations, $\overline{u'_k w'_i w'^i}$ contains not only the second correlations of turbulent velocity, but also the cross- correlations of turbulent velocity and temperature. For simplicity, omitting the non-corresponding second correlations, we get a simplified time-dependent equation for triple correlations:

$$\frac{D \overline{u'_k w'_i w'^i}}{Dt} + \overline{u'_k w'_i w'^i} = -xl \nabla_k \overline{w'_i w'^i} = -3xl \nabla_k x^2. \quad (21)$$

In our calculation of the solar radial p-modes oscillations (Cheng and Xiong, 1997), a set of formulae similar to Eq. (21) had been used to treat all triple correlations ($\overline{u'_k T'^2 / T^2}$ and $\overline{u'_k w'^i T' / T}$). But the results are just contrary to our expectation: The strong spatial oscillations of the convective and related thermal variables existed persistently.

For radial pulsation, Eqs. (19) and (21) can be rewritten as follows

$$\begin{aligned} & \frac{3}{2} \frac{Dx^2}{Dt} - \frac{x^2}{\rho} \frac{D\rho}{Dt} - BV \left\{ \frac{GM_r}{r^2} \left[1 - \frac{\tau_c}{4} \frac{\partial}{\partial \ln r} \left(\frac{u_r}{r} \right) + \frac{Du_r}{Dt} \right] \right\} \\ & + 3 \frac{\partial L_1}{\partial M_r} + 2\sqrt{3} \eta_e \frac{GM_r \rho}{c_1 r^2 P} x^3 = 0, \end{aligned} \quad (22)$$

$$\tau_c \left[\frac{DL_1}{Dt} - L_1 \frac{D \ln(\rho r^2)}{Dt} \right] + L_1 = - \frac{4\sqrt{3} \pi^2 c_2 \rho P r^6 x^3}{GM_r} \frac{\partial \ln x}{\partial M_r}, \quad (23)$$

where $3L_1 = 2\pi r^2 \overline{\rho u'^1 w'_i w'^i}$ is the turbulent kinetic energy flux. In the region where $\omega_r \tau_c \gg 1$, the convective variables x and V change much faster than r , ρ , T and P of the average fluid fields. Therefore, under the first approximation for the purpose of studying the asymptotic properties of

the convective variables, we can ignore the slow variations of r , ρ , P and T of the fluid fields, and simply take them as constants. Bearing this in mind and linearizing Eqs. (22) and (23), we have the following approximated and linearized equations of pulsation,

$$\begin{aligned} & \frac{\sqrt{3}c_2Px^3}{4GM_r\rho} \frac{d \ln x}{d \ln r} \frac{d}{d \ln r} \left(\frac{\delta L_1}{L_1} \right) + \frac{1}{\rho r^3} \frac{\delta L_1}{L_1} \frac{d}{d \ln r} \left(\frac{\sqrt{3}c_2r^3Px^3}{4GM_r} \frac{d \ln x}{d \ln r} \right) \\ & - \frac{GM_r}{r^2} \left[\sqrt{3}\eta_e (2 + i\omega\tau_c) \frac{\rho x^3}{c_1P} \frac{\delta x}{x} - \frac{1}{3}BV \frac{\delta V}{V} \right] = 0, \end{aligned} \quad (24)$$

$$\frac{\sqrt{3}\pi c_2r^3Px^3}{GM_r} \left\{ \frac{d}{d \ln r} \left(\frac{\delta x}{x} \right) + \frac{d \ln x}{d \ln r} \left[3 \frac{\delta x}{x} - (1 + i\omega\tau_c) \frac{\delta L_1}{L_1} \right] \right\} = 0. \quad (25)$$

Besides the convective variables $\delta x/x$ and $\delta L_1/L_1$, Eq. (24) still contains another convective variable $\delta V/V$. Its linearized equation will have other variables, namely $\delta x/x$ and $\delta Z/Z$, where $Z = \overline{T'^2}/\bar{T}^2$ represents the auto-correlation of the turbulent temperature fluctuation. In this case, the three auto- and self-correlations of the fluctuations of turbulent velocity and temperature are closely coupled. We have to solve the 6 linear differential equations for the asymptotic solutions, and this is an extremely difficult procedure. Without losing any generality, we will omit the terms containing the non-diagonal element $\delta V/V$ in Eq. (24) when we discuss Eqs. (25) and (24). Replacing the variable with $\eta = \ln P$, the two equations can be simplified as

$$\frac{dY_1}{d\eta} + \alpha [3Y_1 - (1 + i\omega\tau_c)Y_2] = 0, \quad (26)$$

$$\frac{dY_2}{d\eta} + \left(3\alpha + \frac{d \ln \rho}{d\eta} + 2 \frac{d \ln r}{d\eta} \right) Y_2 - \frac{4\eta_e}{c_1c_2\alpha} (2 + i\omega\tau_c) Y_1 = 0, \quad (27)$$

where

$$\alpha = \frac{d \ln x}{d \ln P}, \quad Y_1 = \frac{\delta x}{x}, \quad Y_2 = \frac{\delta L_1}{L_1}. \quad (28)$$

Neglecting the variation of ρr^2 in space and making the variable conversion

$$Y_2 = \sqrt{\frac{4\eta_e}{c_1c_2} \frac{2 + i\omega\tau_c}{1 + i\omega\tau_c}} \frac{1}{\alpha} X = \frac{\beta}{\alpha} X, \quad (29)$$

Eqs. (26) and (27) can be written as

$$\frac{dY_1}{d\eta} + 3\alpha Y_1 - \beta\sqrt{(1+i\omega\tau_c)(2+i\omega\tau_c)}X = 0, \quad (30)$$

$$\frac{dX}{d\eta} + 3\alpha X - \beta\sqrt{(1+i\omega\tau_c)(2+i\omega\tau_c)}Y_1 = 0. \quad (31)$$

The characteristic values for Eqs. (27) and (28) are

$$\lambda_{\pm} = -3\alpha \pm \beta\sqrt{(1+i\omega\tau_c)(2+i\omega\tau_c)} \approx -3\alpha \pm \left(\frac{3}{2} + i\omega\tau_c\right)\beta, \quad (32)$$

and their general solutions are

$$Y_1 = a_1 P^{-3\alpha + \frac{3}{2}\beta} \cos(\beta\omega\tau_c\eta + \phi_1) + a_2 P^{-3\alpha - \frac{3}{2}\beta} \cos(\beta\omega\tau_c\eta + \phi_2), \quad (33)$$

$$Y_2 = \frac{\beta}{\alpha} \left[a_1 P^{-3\alpha + \frac{3}{2}\beta} \cos(\beta\omega\tau_c\eta + \phi_1) - a_2 P^{-3\alpha - \frac{3}{2}\beta} \cos(\beta\omega\tau_c\eta + \phi_2) \right], \quad (34)$$

where a_1 , a_2 , ϕ_1 and ϕ_2 are constants. Apparently, the solutions Eqs. (33) and (34) are of the oscillating type, and the wavelength of the spatial oscillation is

$$\frac{2\pi}{\beta\omega\tau_c} H_P \approx 4.68 \frac{\sqrt{c_1 c_2}}{\omega\tau_c}. \quad (35)$$

Within the convective overshooting zone, it follows from the asymptotic properties of convective overshooting (Xiong, 1989) that

$$\alpha \approx \pm \sqrt{\frac{1 + 2\sqrt{3}\eta_e}{3\sqrt{3}c_1 c_2}} = \pm \frac{0.70175}{\sqrt{c_1 c_2}}. \quad (36)$$

In the upper overshooting zone of a convective region, α is the positive solution. To avoid a too fast outwards growing amplitude, we choose $\lambda = \lambda_+$, i.e. we take $a_2 = 0$ in Eqs. (33) and (34). On the other hand, in the lower overshooting zone of a convective region, where $\alpha < 0$, we take $\lambda = \lambda_-$, i.e. $a_1 = 0$.

According to Eqs. (29), (33), (34) and (36), the convective variables tend to have an oscillating solution with a growing amplitude towards convective overshooting zone, the e-folding length of which is

$$\left| -3\alpha \pm \frac{3}{2}\beta \right| = \frac{0.09278}{\sqrt{c_1 c_2}} H_P. \quad (37)$$

There exist the similar spatial oscillating behavior as above for the auto-correlation of temperature fluctuation Z and the cross-correlation V of velocity and temperature fluctuations. The procedure to follow is also the same as described above, so we will not go into their details.

Now, it is not difficult to understand why there exist intense spatial oscillations in the region where $\omega_r\tau_c \gg 1$. Let's look back at Eq. (21). The triple correlations $\overline{u'_\alpha w'_i w'^i}$ must approach to zero when $\omega_r\tau_c \gg 1$. That is to say, the nonlocal convection theory approaches to the local one. Thus the spatial oscillations occurring in the calculation of local convection theory will certainly come out. To avoid spatial oscillations, we go back to the simple gradient type diffusion approximation respectively by Eq. (20). The corresponding linear pulsational equation becomes

$$\frac{dY_1}{d\eta} + 3\alpha Y_1 - \alpha Y_2 = 0. \quad (38)$$

Making a new variable conversion

$$Y_2 = \sqrt{\frac{4\eta_e}{c_1 c_2} (2 + i\omega\tau_c)} \frac{1}{\alpha} X = \frac{\beta_1}{\alpha} X, \quad (39)$$

Eqs. (38) and (27) can be written as

$$\frac{dY_1}{d\eta} + 3\alpha Y_1 - \beta_1 \sqrt{2 + i\omega\tau_c} X = 0, \quad (40)$$

$$\frac{dX}{d\eta} + 3\alpha X - \beta_1 \sqrt{2 + i\omega\tau_c} Y_1 = 0. \quad (41)$$

Their characteristic values are

$$\lambda'_\pm = 3\alpha \pm \sqrt{2 + i\omega\tau_c} \beta_1 = 3\alpha \pm \sqrt{2} \beta_1 (\cos \phi + i \sin \phi), \quad (42)$$

where $2\phi = \arctan \frac{\omega\tau_c}{2}$. It is clear that if $\omega\tau_c \rightarrow \infty$, we have $\phi \rightarrow \pi/4$. Therefore, in the upper overshooting zone where $\alpha > 0$, we chose the solution with $\lambda = \lambda'_+$; while in the bottom overshooting zone where $\alpha < 0$ we chose the solution with $\lambda = \lambda'_-$. Then the spatial oscillations become solutions attenuating rapidly towards the overshooting zone. By doing so, we restrained effectively the spatial oscillations in our calculations. The trace of spatial oscillations of eigen-functions can still be found in the outmost zones where $\omega\tau_c \gg 1$ in Fig. 1, and especially for convection variables (y_5 – y_{10}). The eigen-function of turbulent velocity in the outmost stellar zones is plotted on Fig. 1f, where the spatial oscillations are very clear.

These asymptotic solutions were used as the convective boundary conditions at the top and bottom in the numerical calculations of non-adiabatic oscillations.

4. Discussion and Conclusions

We have carried out theoretical calculations of linear non-adiabatic oscillations for six series of HB stellar models. The main results can be summarized in the following,

1. When the coupling between convection and oscillations is ignored, it is not possible to interpret the red edge of the RR Lyrae instability strip. All the HB models with $T_e \leq 6200K$ are pulsationally unstable from the fundamental up to (at least) the 9th overtone;
2. The intrinsic reason for the existence of the red edge of the RR instability strip is the coupling between convection and oscillations. Our numerical results show that, when taking the coupling into consideration, all the low temperature HB models with $T_e \leq 5940K$ have pulsationally stable fundamental and low-order overtones ($n \leq 3$). The turbulent viscosity is an important damping mechanism of oscillations.
3. For the low temperature red HB star models some of the high-order overtones ($n \geq 4$) become pulsationally unstable. The pulsational periods of these high-order overtones are of the order of a few tenths of a day. This might be the clue for the red variables outside the RR Lyrae instability strip in globular clusters found by Yao and his collaborators (Yao, 1981, 1986, 1987; Yao et al. 1993a,b, 1994).
4. The pulsational properties of RHBS are very different from those of LRV. In the current works, all low temperature red models with $T_e \leq 5940K$ have pulsationally unstable fundamental and the low-order overtones ($n \leq 3$), while some of their high-order overtones ($n \geq 4$) are pulsationally unstable. Opposite to this, the LRV outside the Cepheid instability strip (i.e. the long period variables) are pulsationally stable for all the high-order overtones ($n \geq 4$), while the fundamental and the first overtone are possibly unstable. The tremendous difference of mass-luminosity ratios is the reason for the distinct properties of the two types of low temperature variables.
5. The spatial oscillations of the convective and the thermal variables in the local time-dependent convection theory are effectively restrained in the present paper, where a nonlocal time-dependent convection theory is used to treat the coupling between convection and oscillations.

Comparing Tables 2 and 3 we have found that, the effects of convection on the instability of such stars still cannot be ignored for the blue HB stars ($T_e \geq 7000K$), although the convective envelope is already very shallow and the convective energy transport becomes negligible ($L_c/L \ll 1$). These effects are mainly due to the dynamic coupling between convection and oscillations, other than the thermodynamic coupling, because in the outermost layer of the blue HB stars, a certain amount of turbulent pressure remains, even if the convective energy transport is negligible there. We made a numerical test, in which the dynamic coupling was ignored. The

results show that all the low-order overtones become pulsationally stable. We are reluctant to draw any further conclusion on the pulsational properties of the blue HB stars because there are some undetermined factors, i.e.

1. There are spatial oscillations in the stellar atmosphere (Fig. 1f). We cannot estimate quantitatively their influence on the results of numerical calculations. Their effect, we think, may be unimportant to the cool RHBS, because they have extended convective envelopes. There are no any spatial oscillations in the main part of the convective zone except the atmosphere (Fig. 1). However, convection appears only in a limited surface region and the pulsational stability coefficient is small for the blue HB stars. The spatial oscillations become, maybe, more important in comparison with the RHBS.
2. The undetermined structure of the turbulent atmosphere of stars. The atmosphere has an unnegligible influence on the pulsational stability of stars, especially for the blue HB stars, which have small pulsational stability. It is very difficult to construct an exact enough model of turbulent atmosphere.

This problem deserves future investigation. The high-precision photometry of variables is available for us to determine whether there are low-order unstable modes in the blue HB stars.

The present work is supported in part by the contract 19573018 of the National Natural Science Foundation of China(NSFC).

REFERENCES

- Alexander, D.R., 1975, ApJS, 29, 363
- Baker, N.H. & Gough, D.O., 1979, ApJ, 234, 232
- Balmforth, N.J. & Gough, D.O., 1987, in *Seismology of the Sun and Sun-like Stars*, ed. Rolfe, E. (ESA sp-286), p. 47
- Bono, G. & Stellingwerf, R.F., 1993, ApJS, 93, 233
- Bono, G., Caputo, F., Castellani, V. Marconi, L.M., Stalano, L. & Stellingwerf, R.F., 1995, ApJ, 442, 159
- Bono, G., Caputo, F., Castellani, V. & Marconi, L.M., 1997, ApJS, 121, 327
- Cheng, Q.L. & Xiong, D.R., 1997, A&A 319, 981
- Christy, R.F., 1966, ApJ, 144, 108
- Dappen, W., Mihalas, D., Hummer, D.G. & Mihalas, b.W., 1988, ApJ, 332, 261
- Deupree, R.G., 1977a, ApJ, 211, 509

- Deupree, R.G., 1977b, *ibid*, 214, 502
Deupree, R.G., 1977c, *ibid*, 215, 232
Gonczi, G., & Osaki, Y., 1980, *A&A*, 84, 196
Gough, D.O., 1977, *ApJ*, 214, 196
Guzik, J.A. & Cox, A.N., 1993, *Astrophys. Spac. Sci.*, 210, 307
Henyey, L.G., Forbes, J.E. & Gould, N.L., 1964, *ApJ*, 139, 306
Hummer, D.G. & Mihalas, D., 1988, *ApJ*, 331, 794
Iben, I.Jr., 1971, *ApJ*, 166, 131
Keeley, D.A., 1977, *ApJ*, 221, 926
Mihalas, D., Dappen, W. & Hummer, D.G., 1988, *ApJ*, 331, 815
Rogers, F. & Iglesias, C.A., 1992, *ApJS*, 79, 507
Sandage, A.R., 1990, *ApJ*, 350, 603
Stellingwerf, R.F., 1984, *ApJ*, 277, 322
Vitense, E., 1958, *Z. Astrophys.*, 46, 108
Xiong, D.R., 1977, *Acta Astron. Sinica*, 18, 86 (English Tran. in *Chinese Astronomy*, 2, 118)
Xiong, D.R., 1979, *Acta Astron. Sinica*, 20, 238 (English Tran. in *Chinese Astronomy*, 4, 234)
Xiong, D.R., 1980, *Scientia Sinica*, 23 1139
Xiong, D.R., 1989, *A&A*, 209, 126
Xiong, D.R., Cheng, Q.L. & Deng L., 1997 *ApJS*, 108, 529
Xiong, D.R., Deng, L. & Cheng, Q.L., 1997 submitted to *ApJ*
Yao, B.A., 1981, *Acta Astrophys. Sinica*, 1, 311
Yao, B.A., 1986, *Astrophys. Spac. Sci.*, 119, 41
Yao, B.A., 1987, *ESO Messenger*, No. 50, 33
Yao, B.A., Zhang, C.S. & Qin, D., 1993a, *IBVS*, No. 3955
Yao, B.A., Zhang, C.S. & Qin, D., 1993b, *IBVS*, No. 3962
Yao, B.A., Zhang, C.S. & Qin, D., 1994, *IBVS*, No. 4003

Figure Captions

Fig. 1.— The normalized eigen-functions of the 10th overtone for the coldest HB star model in series 2.

Fig. 2.— The integrated work W_P versus depth for six different HB star models. The coupling between convection and oscillations is ignored. W_{KM} and W_{RME} are respectively the contribution components of the κ mechanism (KM) and radiative modulation excitation (RME). The radiative energy flux L_r/L , the adiabatic index Γ_2 , and the partial differential of opacity with respect to temperature, χ_T are also plotted. Three horizontal lines indicate the locations of the ionization regions of H and He.

Fig. 3.— The variation of the growth rates of the fundamental and the first overtone versus effective temperature for three model series of HB stars. The solid and long-dashed lines show the cases with consideration of the coupling between convection and oscillations (WCC), while the dotted and the dot-dashed lines shows the cases ignoring the convection coupling (W - OCC).

Fig. 4.— The same as Fig. 2, but the coupling between convection and oscillations is considered. W_P , W_{Pt} and W_{vis} are, respectively, the contributions due to gas (and radiation) pressure, turbulent pressure and turbulent viscosity, while W_{all} is the total integrated work, the other symbols are the same as in Fig. 2.

Fig. 5.— The integrated work virsus depth for the first, second, and fourth overtones of a $T_e = 5150K$ HB star model, the coupling between convection and oscillations is considered. Refer to Fig. 4 for details.

Fig. 6.— The bottom temperatures of the hydrogen, the first and the second helium ionization regions and convective region versus effective temperature for the model series 2 of HB stars. The horizontal lines are the location of the RR Lyrae instability strip. The horizontal line indicates the locations of the RR Lyrae instability sttip.

Fig. 7.— The variation of radius r , mass M_r and the local pressure scale height H_P versus depth ($\log T$). Panel a.: the envelope model of a HB star with $T_e = 5300K$; Panel b.: a long period variable envelope model with $M = 1M_\odot$, $L = 5000L_\odot$, $T_e = 2700K$, $x = 0.70$ and $z = 0.020$.

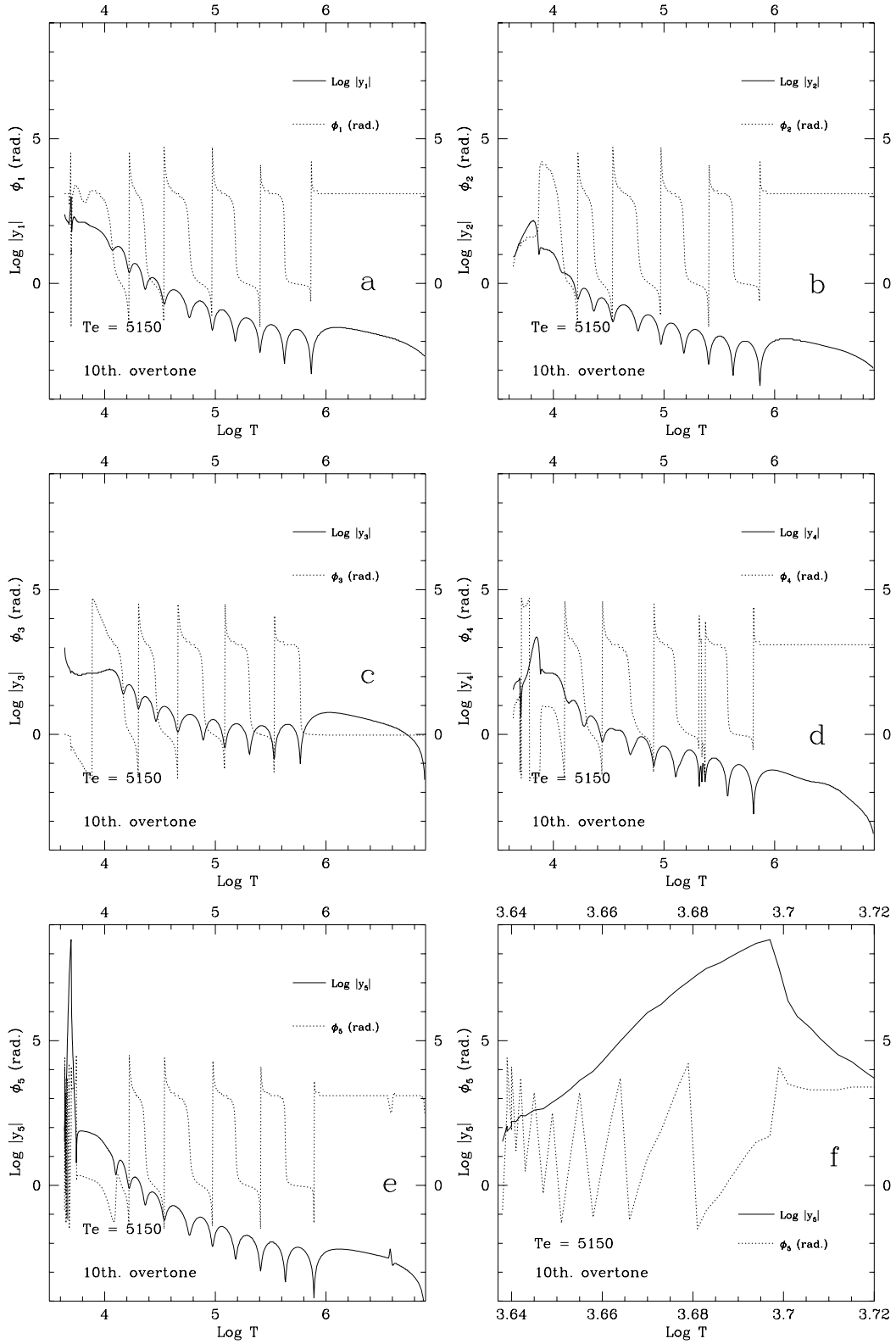


Fig. 1.—

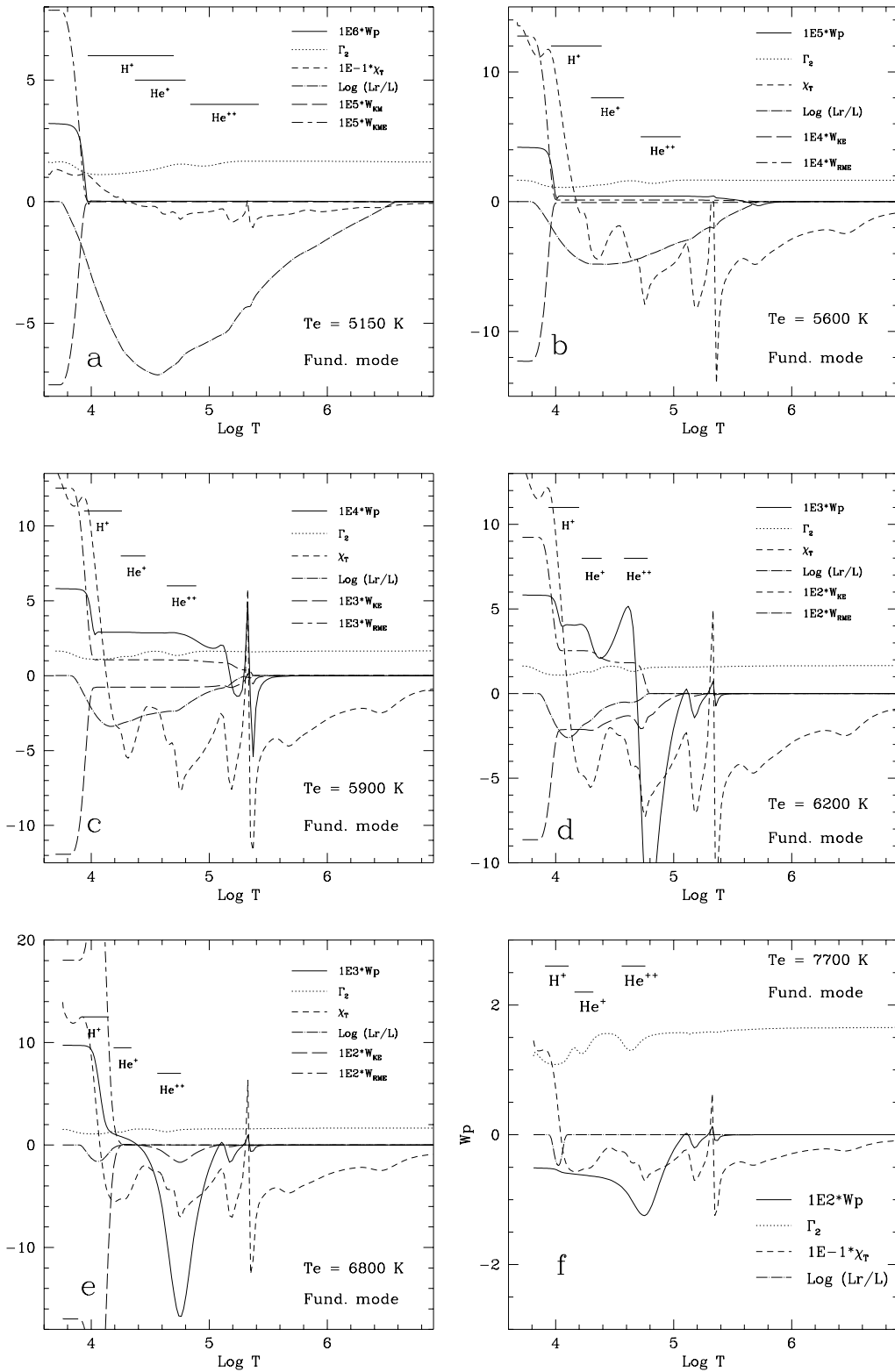


Fig. 2.—

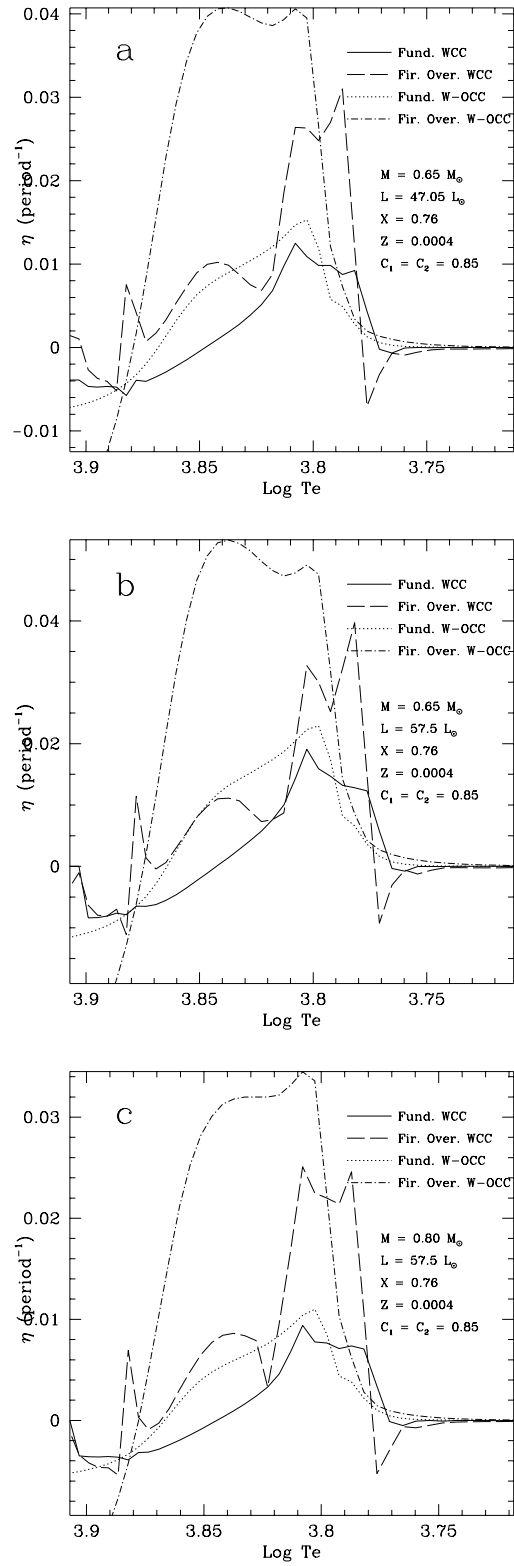


Fig. 3.—

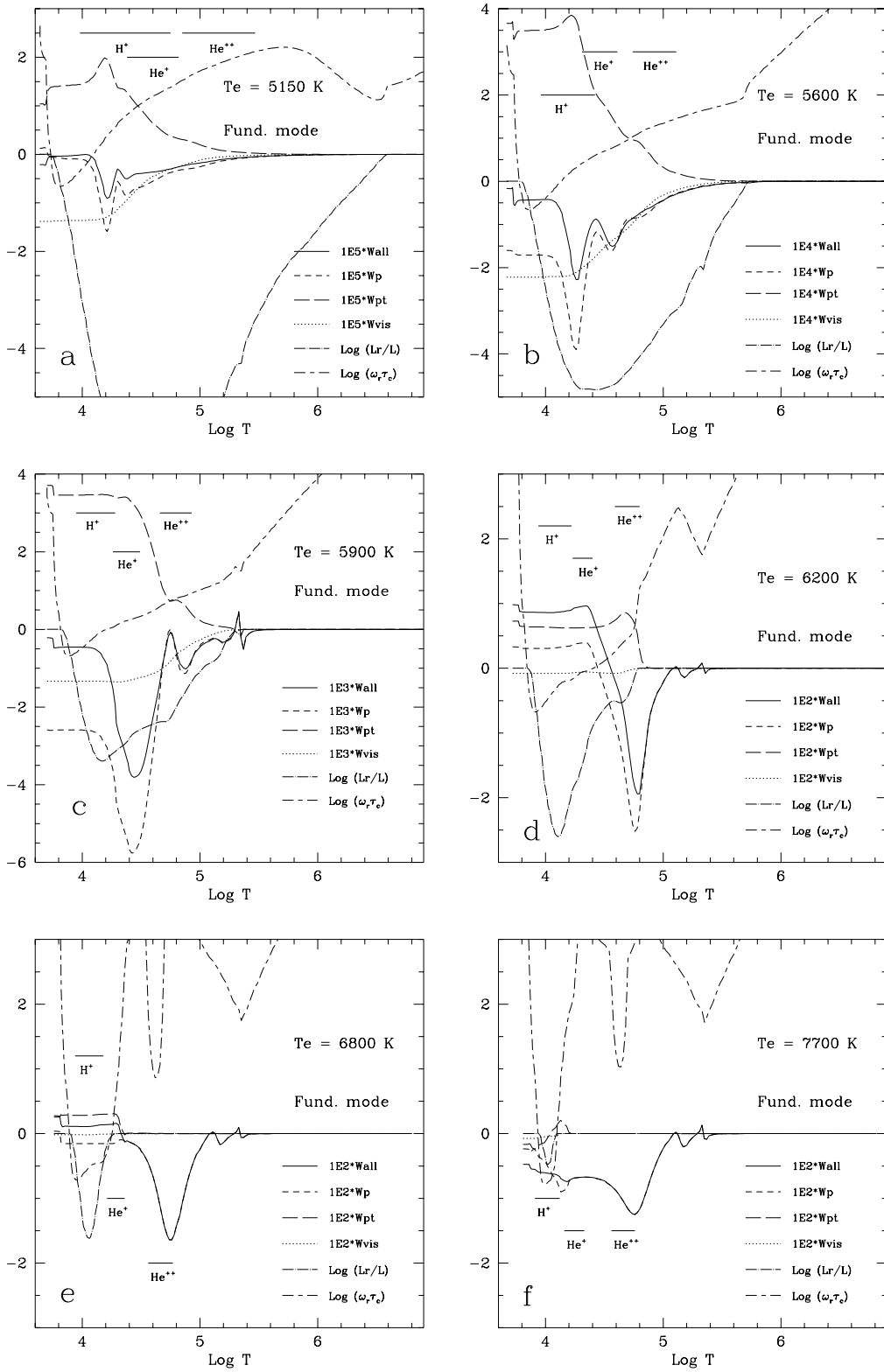


Fig. 4.—

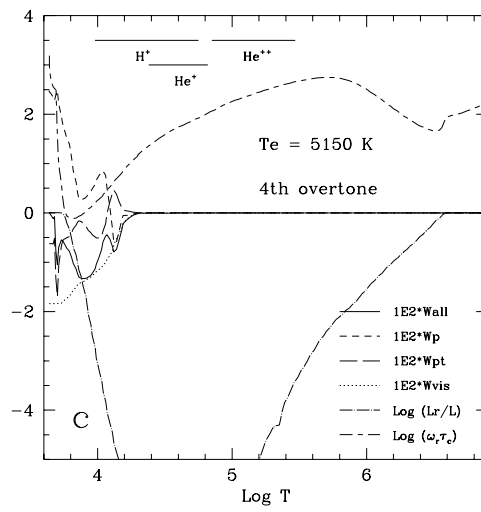
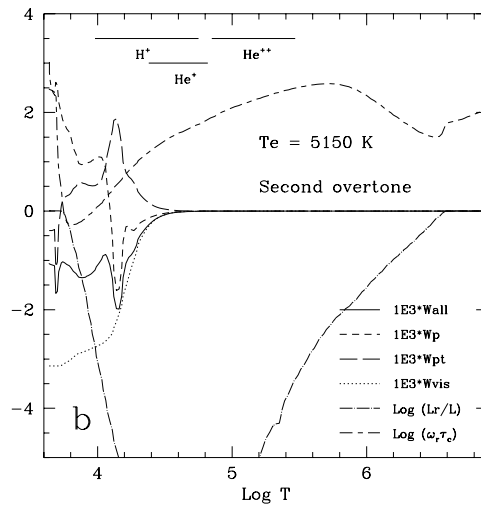
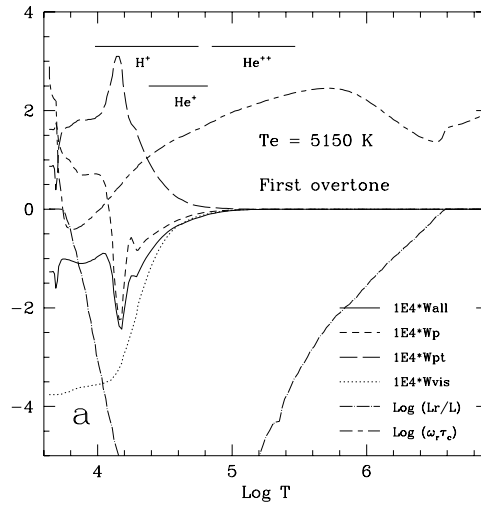


Fig. 5.—

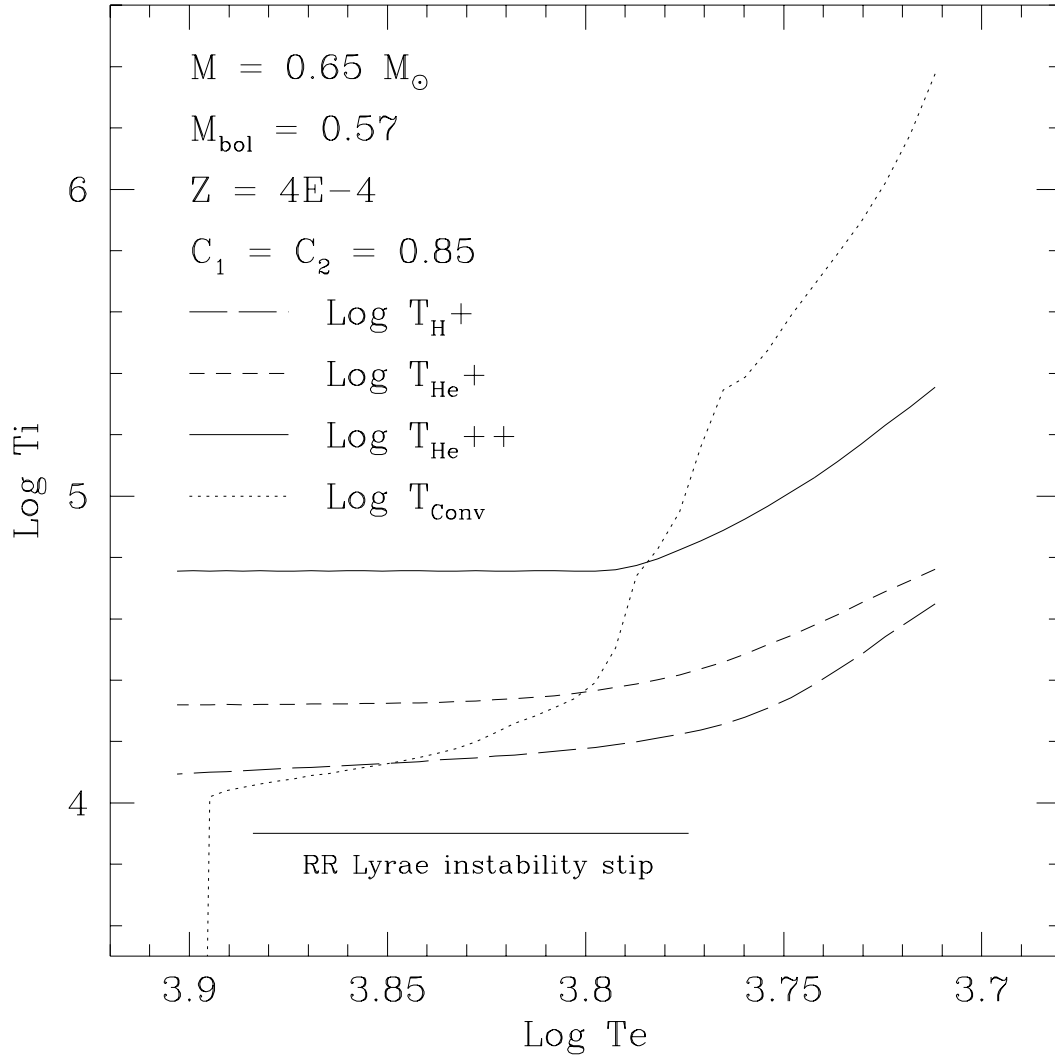


Fig. 6.—

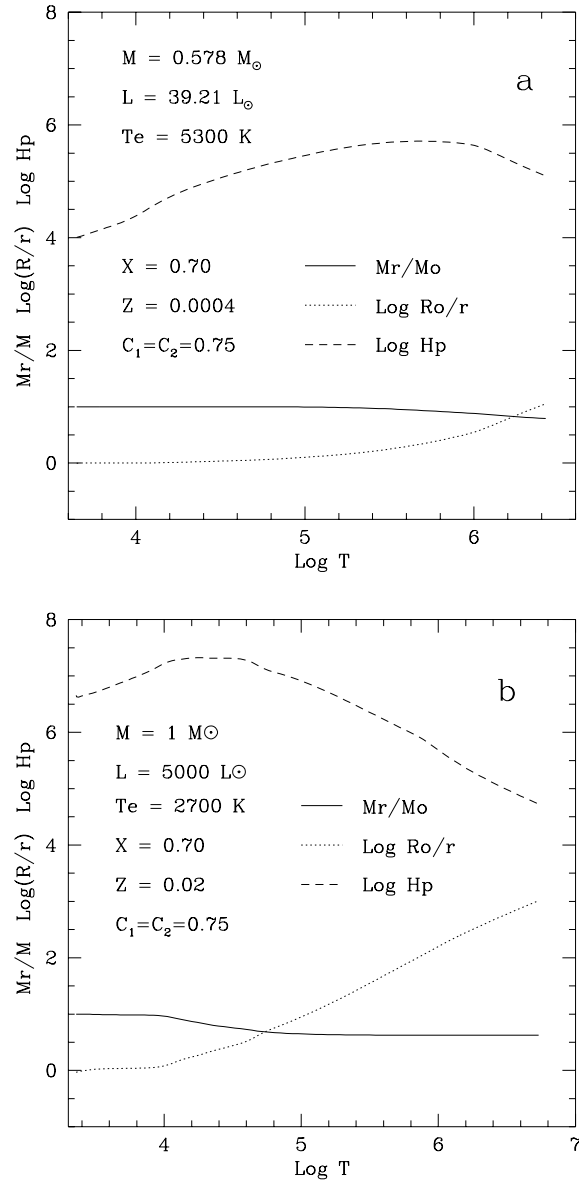


Fig. 7.—

Table 1. Pulsational instability strip (PIS)
 $X = 0.76, Z = 0.0004$

no	M/M_{\odot}	L/L_{\odot}	$c_1 = c_2$	pulsational instability strip	
				F-mode	1st overtone
1	0.65	39.2	0.85	5940 - 7140K	6090 - 7660K
2	0.65	47.1	0.85	5940 - 7060K	6010 - 7660K
3	0.65	57.5	0.85	5860 - 6990K	5940 - 7590K
4	0.80	57.5	0.85	5940 - 6990K	6010 - 7360K
5	0.65	47.1	0.75	5790 - 6990K	5860 - 7510K
6	0.65	47.1	1.00	6010 - 7060K	6160 - 7440K

Table 2. Amplitude growth rates for the first 12 modes
 $M = 0.65M_{\odot}$, $L = 47.047L_{\odot}$, $X=0.76$, $Z=0.0004$

no	Te	η_0	η_1	η_2	η_3	η_4	η_5	η_6	η_7	η_8	η_9
1	5150.0	0.32D-05	0.58D-04	0.57D-03	0.16D-02	0.33D-02	0.39D-02	0.44D-02	0.38D-02	0.28D-02	0.10D-02
2	5225.0	0.50D-05	0.81D-04	0.72D-03	0.19D-02	0.38D-02	0.44D-02	0.50D-02	0.43D-02	0.34D-02	0.15D-02
3	5300.0	0.75D-05	0.11D-03	0.90D-03	0.23D-02	0.44D-02	0.49D-02	0.57D-02	0.51D-02	0.42D-02	0.24D-02
4	5375.0	0.11D-04	0.14D-03	0.11D-02	0.27D-02	0.50D-02	0.55D-02	0.66D-02	0.61D-02	0.53D-02	0.36D-02
5	5450.0	0.17D-04	0.19D-03	0.14D-02	0.32D-02	0.57D-02	0.64D-02	0.74D-02	0.74D-02	0.64D-02	0.51D-02
6	5525.0	0.26D-04	0.26D-03	0.16D-02	0.38D-02	0.62D-02	0.75D-02	0.80D-02	0.88D-02	0.78D-02	0.66D-02
7	5600.0	0.42D-04	0.35D-03	0.20D-02	0.46D-02	0.65D-02	0.89D-02	0.86D-02	0.10D-01	0.96D-02	0.81D-02
8	5675.0	0.72D-04	0.49D-03	0.23D-02	0.54D-02	0.67D-02	0.10D-01	0.99D-02	0.11D-01	0.11D-01	0.10D-01
9	5750.0	0.13D-03	0.70D-03	0.25D-02	0.63D-02	0.73D-02	0.11D-01	0.12D-01	0.11D-01	0.12D-01	0.12D-01
10	5825.0	0.27D-03	0.97D-03	0.28D-02	0.70D-02	0.88D-02	0.10D-01	0.14D-01	0.13D-01	0.13D-01	0.13D-01
11	5900.0	0.58D-03	0.14D-02	0.30D-02	0.74D-02	0.11D-01	0.10D-01	0.14D-01	0.16D-01	0.15D-01	0.14D-01
12	5975.0	0.13D-02	0.20D-02	0.36D-02	0.71D-02	0.12D-01	0.12D-01	0.13D-01	0.17D-01	0.18D-01	0.16D-01
13	6050.0	0.28D-02	0.34D-02	0.43D-02	0.65D-02	0.12D-01	0.14D-01	0.13D-01	0.14D-01	0.18D-01	0.18D-01
14	6125.0	0.49D-02	0.73D-02	0.54D-02	0.51D-02	0.98D-02	0.14D-01	0.14D-01	0.11D-01	0.12D-01	0.15D-01
15	6200.0	0.58D-02	0.12D-01	0.77D-02	0.21D-02	0.24D-02	0.73D-02	0.10D-01	0.68D-02	0.22D-02	0.11D-02
16	6275.0	0.12D-01	0.27D-01	0.16D-01	0.15D-02	-0.81D-02	-0.10D-01	-0.54D-02	-0.42D-02	-0.11D-01	-0.21D-01
17	6350.0	0.15D-01	0.39D-01	0.24D-01	0.17D-02	-0.16D-01	-0.26D-01	-0.27D-01	-0.28D-01	-0.32D-01	-0.44D-01
18	6425.0	0.15D-01	0.41D-01	0.21D-01	-0.71D-02	-0.30D-01	-0.44D-01	-0.51D-01	-0.59D-01	-0.67D-01	-0.82D-01
19	6500.0	0.13D-01	0.39D-01	0.17D-01	-0.17D-01	-0.46D-01	-0.66D-01	-0.79D-01	-0.95D-01	-0.11D+00	-0.13D+00
20	6575.0	0.12D-01	0.39D-01	0.16D-01	-0.24D-01	-0.58D-01	-0.81D-01	-0.97D-01	-0.12D+00	-0.14D+00	-0.16D+00
21	6650.0	0.11D-01	0.39D-01	0.17D-01	-0.26D-01	-0.62D-01	-0.87D-01	-0.10D+00	-0.13D+00	-0.14D+00	-0.15D+00
22	6725.0	0.10D-01	0.40D-01	0.20D-01	-0.25D-01	-0.63D-01	-0.87D-01	-0.11D+00	-0.13D+00	-0.14D+00	-0.14D+00
23	6800.0	0.97D-02	0.40D-01	0.23D-01	-0.22D-01	-0.61D-01	-0.86D-01	-0.11D+00	-0.13D+00	-0.14D+00	-0.12D+00
24	6875.0	0.90D-02	0.41D-01	0.27D-01	-0.18D-01	-0.59D-01	-0.84D-01	-0.11D+00	-0.13D+00	-0.13D+00	-0.10D+00
25	6950.0	0.83D-02	0.41D-01	0.30D-01	-0.16D-01	-0.58D-01	-0.85D-01	-0.11D+00	-0.13D+00	-0.12D+00	-0.88D-01
26	7025.0	0.74D-02	0.40D-01	0.33D-01	-0.14D-01	-0.60D-01	-0.88D-01	-0.11D+00	-0.13D+00	-0.11D+00	-0.72D-01
27	7100.0	0.63D-02	0.38D-01	0.34D-01	-0.14D-01	-0.64D-01	-0.96D-01	-0.12D+00	-0.13D+00	-0.92D-01	-0.55D-01
28	7175.0	0.49D-02	0.34D-01	0.33D-01	-0.17D-01	-0.72D-01	-0.11D+00	-0.13D+00	-0.12D+00	-0.74D-01	-0.39D-01
29	7250.0	0.32D-02	0.29D-01	0.29D-01	-0.22D-01	-0.83D-01	-0.12D+00	-0.14D+00	-0.10D+00	-0.56D-01	-0.23D-01
30	7325.0	0.14D-02	0.23D-01	0.23D-01	-0.30D-01	-0.99D-01	-0.14D+00	-0.14D+00	-0.86D-01	-0.40D-01	-0.92D-02
31	7400.0	-0.40D-03	0.16D-01	0.16D-01	-0.40D-01	-0.12D+00	-0.16D+00	-0.14D+00	-0.69D-01	-0.27D-01	0.13D-02
32	7475.0	-0.20D-02	0.83D-02	0.66D-02	-0.51D-01	-0.14D+00	-0.17D+00	-0.12D+00	-0.57D-01	-0.19D-01	0.71D-02
33	7550.0	-0.33D-02	0.17D-02	-0.21D-02	-0.61D-01	-0.15D+00	-0.17D+00	-0.11D+00	-0.50D-01	-0.17D-01	0.73D-02
34	7625.0	-0.43D-02	-0.39D-02	-0.97D-02	-0.68D-01	-0.15D+00	-0.16D+00	-0.10D+00	-0.47D-01	-0.19D-01	0.26D-02
35	7700.0	-0.51D-02	-0.86D-02	-0.16D-01	-0.72D-01	-0.15D+00	-0.15D+00	-0.92D-01	-0.47D-01	-0.26D-01	-0.66D-02
36	7775.0	-0.57D-02	-0.12D-01	-0.21D-01	-0.73D-01	-0.15D+00	-0.14D+00	-0.86D-01	-0.48D-01	-0.32D-01	-0.16D-01
37	7850.0	-0.62D-02	-0.16D-01	-0.26D-01	-0.73D-01	-0.14D+00	-0.13D+00	-0.82D-01	-0.51D-01	-0.39D-01	-0.24D-01
38	7925.0	-0.66D-02	-0.18D-01	-0.30D-01	-0.73D-01	-0.13D+00	-0.12D+00	-0.79D-01	-0.53D-01	-0.46D-01	-0.32D-01
39	8000.0	-0.69D-02	-0.21D-01	-0.33D-01	-0.72D-01	-0.13D+00	-0.11D+00	-0.77D-01	-0.55D-01	-0.51D-01	-0.39D-01
40	8075.0	-0.72D-02	-0.23D-01	-0.37D-01	-0.71D-01	-0.12D+00	-0.11D+00	-0.76D-01	-0.58D-01	-0.57D-01	-0.46D-01

Table 3. Amplitude growth rates for the first 12 modes
 $M = 0.65M_{\odot}$, $L = 47.047L_{\odot}$, $X=0.76$, $Z=0.0004$

no	Te	η_0	η_1	η_2	η_3	η_4	η_5	η_6	η_7	η_8	η_9
1	5150.0	-0.21D-05	-0.13D-03	-0.11D-02	-0.19D-02	0.18D-03	0.92D-02	0.26D-01	0.45D-01	0.62D-01	0.67D-01
2	5225.0	-0.25D-05	-0.15D-03	-0.14D-02	-0.39D-02	-0.77D-02	-0.81D-02	-0.49D-02	0.48D-02	0.18D-01	0.28D-01
3	5300.0	-0.22D-05	-0.16D-03	-0.14D-02	-0.39D-02	-0.90D-02	-0.12D-01	-0.15D-01	-0.12D-01	-0.43D-02	0.58D-02
4	5375.0	-0.20D-05	-0.18D-03	-0.14D-02	-0.37D-02	-0.85D-02	-0.12D-01	-0.17D-01	-0.17D-01	-0.13D-01	-0.42D-02
5	5450.0	-0.20D-05	-0.18D-03	-0.12D-02	-0.32D-02	-0.71D-02	-0.11D-01	-0.15D-01	-0.17D-01	-0.14D-01	-0.80D-02
6	5525.0	-0.77D-05	-0.20D-03	-0.10D-02	-0.26D-02	-0.50D-02	-0.82D-02	-0.11D-01	-0.14D-01	-0.13D-01	-0.83D-02
7	5600.0	-0.16D-04	-0.29D-03	-0.12D-02	-0.84D-03	-0.13D-02	-0.46D-02	-0.70D-02	-0.99D-02	-0.10D-01	-0.63D-02
8	5675.0	-0.13D-04	-0.57D-03	-0.63D-03	-0.36D-03	-0.71D-03	-0.23D-02	-0.39D-02	-0.50D-02	-0.50D-02	-0.25D-02
9	5750.0	-0.65D-04	-0.89D-03	-0.19D-02	-0.13D-02	-0.17D-03	0.65D-04	0.32D-05	-0.65D-04	0.56D-03	0.21D-02
10	5825.0	-0.66D-03	-0.69D-03	-0.31D-02	-0.54D-02	-0.27D-02	0.59D-03	0.35D-02	0.58D-02	0.65D-02	0.70D-02
11	5900.0	-0.21D-03	-0.32D-02	-0.15D-02	-0.70D-02	-0.12D-01	-0.57D-02	0.21D-02	0.10D-01	0.14D-01	0.13D-01
12	5975.0	0.44D-02	-0.70D-02	-0.73D-02	-0.74D-03	-0.33D-02	-0.88D-02	-0.72D-02	0.26D-02	0.17D-01	0.23D-01
13	6050.0	0.92D-02	0.12D-01	-0.14D-01	-0.17D-01	-0.22D-02	0.91D-02	0.11D-01	0.93D-02	0.14D-01	0.23D-01
14	6125.0	0.87D-02	0.31D-01	0.43D-01	0.15D-01	-0.10D-01	0.36D-02	0.33D-01	0.40D-01	0.33D-01	0.30D-01
15	6200.0	0.98D-02	0.27D-01	0.41D-01	0.63D-01	0.90D-01	0.71D-01	0.61D-01	0.82D-01	0.81D-01	0.58D-01
16	6275.0	0.98D-02	0.25D-01	0.23D-01	0.20D-01	0.23D-01	0.31D-01	0.31D-01	0.53D-01	0.15D+00	0.13D+00
17	6350.0	0.11D-01	0.26D-01	0.14D-01	-0.26D-02	-0.18D-01	-0.31D-01	-0.47D-01	-0.76D-01	-0.13D+00	-0.44D-01
18	6425.0	0.13D-01	0.26D-01	0.43D-02	-0.25D-01	-0.53D-01	-0.77D-01	-0.11D+00	-0.14D+00	-0.15D+00	-0.10D+00
19	6500.0	0.98D-02	0.18D-01	-0.21D-01	-0.76D-01	-0.14D+00	-0.22D+00	-0.68D+00	-0.26D+00	-0.12D+00	-0.67D-01
20	6575.0	0.68D-02	0.88D-02	-0.51D-01	-0.11D+00	-0.11D+00	-0.39D-01	0.27D-01	0.57D-01	0.55D-01	0.38D-01
21	6650.0	0.51D-02	0.68D-02	-0.61D-01	-0.14D+00	-0.14D+00	-0.27D-01	0.44D-01	0.79D-01	0.79D-01	0.60D-01
22	6725.0	0.39D-02	0.75D-02	-0.57D-01	-0.21D+00	-0.84D+00	-0.13D+00	-0.25D-01	0.13D-01	0.23D-01	0.15D-01
23	6800.0	0.28D-02	0.87D-02	-0.45D-01	-0.19D+00	-0.47D+00	-0.23D+00	-0.73D-01	-0.27D-01	-0.91D-02	-0.11D-01
24	6875.0	0.19D-02	0.99D-02	-0.32D-01	-0.14D+00	-0.29D+00	-0.22D+00	-0.94D-01	-0.46D-01	-0.25D-01	-0.22D-01
25	6950.0	0.98D-03	0.10D-01	-0.22D-01	-0.11D+00	-0.20D+00	-0.17D+00	-0.90D-01	-0.50D-01	-0.31D-01	-0.27D-01
26	7025.0	0.15D-03	0.10D-01	-0.14D-01	-0.85D-01	-0.15D+00	-0.13D+00	-0.76D-01	-0.46D-01	-0.33D-01	-0.29D-01
27	7100.0	-0.69D-03	0.89D-02	-0.80D-02	-0.67D-01	-0.11D+00	-0.96D-01	-0.59D-01	-0.40D-01	-0.33D-01	-0.30D-01
28	7175.0	-0.15D-02	0.72D-02	-0.42D-02	-0.55D-01	-0.92D-01	-0.74D-01	-0.45D-01	-0.34D-01	-0.33D-01	-0.32D-01
29	7250.0	-0.22D-02	0.53D-02	-0.12D-02	-0.44D-01	-0.75D-01	-0.57D-01	-0.35D-01	-0.30D-01	-0.34D-01	-0.34D-01
30	7325.0	-0.29D-02	0.33D-02	0.12D-02	-0.34D-01	-0.60D-01	-0.44D-01	-0.27D-01	-0.28D-01	-0.36D-01	-0.35D-01
31	7400.0	-0.35D-02	0.17D-02	0.46D-02	-0.23D-01	-0.45D-01	-0.33D-01	-0.23D-01	-0.30D-01	-0.41D-01	-0.36D-01
32	7475.0	-0.41D-02	0.71D-03	0.96D-02	-0.10D-01	-0.29D-01	-0.24D-01	-0.22D-01	-0.36D-01	-0.47D-01	-0.33D-01
33	7550.0	-0.39D-02	0.42D-02	0.24D-01	0.13D-01	-0.74D-02	-0.16D-01	-0.30D-01	-0.54D-01	-0.50D-01	-0.13D-01
34	7625.0	-0.58D-02	0.75D-02	0.18D+00	0.96D-01	-0.24D-01	-0.15D+00	-0.16D+00	-0.40D-01	0.56D-02	0.30D-01
35	7700.0	-0.47D-02	-0.52D-02	-0.49D-02	-0.47D-01	-0.11D+00	-0.13D+00	-0.99D-01	-0.50D-01	-0.20D-01	0.62D-02
36	7775.0	-0.47D-02	-0.41D-02	0.16D-02	-0.34D-01	-0.10D+00	-0.14D+00	-0.12D+00	-0.54D-01	-0.13D-01	0.19D-01
37	7850.0	-0.47D-02	-0.37D-02	0.66D-02	-0.23D-01	-0.92D-01	-0.15D+00	-0.14D+00	-0.56D-01	-0.15D-02	0.34D-01
38	7925.0	-0.47D-02	-0.27D-02	0.13D-01	-0.90D-02	-0.76D-01	-0.15D+00	-0.17D+00	-0.54D-01	0.17D-01	0.55D-01
39	8000.0	-0.39D-02	0.10D-02	0.23D-01	0.39D-02	0.39D-02	-0.68D-01	-0.21D+00	-0.35D-01	0.46D-01	0.62D-01
40	8075.0	-0.39D-02	0.14D-02	0.26D-01	0.14D-01	-0.48D-01	-0.15D+00	-0.21D+00	-0.48D-01	0.34D-01	0.66D-01